

Detection of pulsed γ -rays above 25 GeV from the Crab pulsar

The MAGIC collaboration

(author and affiliation lists appear at the end of this paper)

One fundamental unanswered question about pulsars concerns the mechanism of their pulsed electromagnetic radiation. Measuring the high end region of a pulsar's spectrum would shed light on this question, but has challenged ground-based experiments for three decades. By developing a new type of electronic trigger, we could lower the threshold of the MAGIC Cherenkov telescope to 25 GeV, a major breakthrough for this kind of instrument. We detected pulsed γ -rays from the Crab above 25 GeV, revealing a relatively high energy cut-off in the phase-averaged spectrum. This indicates that emission happens far out in the magnetosphere. Also, the main-pulse and secondary pulse have similar amplitudes at 25 GeV. These results exclude the polar cap model and challenge the slot gap emission model for Crab.

It is generally accepted that the primary radiation mechanism in the magnetosphere of pulsars is inverse Compton scattering and synchrotron-curvature radiation. The latter occurs when relativistic electrons are trapped along the magnetic field lines in the extremely strong field of the pulsar. It is not known whether the emission of electromagnetic radiation takes place closer (*polar cap* scenario (1)) to the neutron star (NS) or farther out in the magnetosphere (*outer gap* scenario (2)), see Fig. 1. The high end of the spectrum differs significantly in the two cases. Therefore, observation of γ -rays above 10 GeV allows one to differentiate among pulsar emission models.

To date, this energy has been out of the range accessible to satellite observations. At $E \approx 1$ GeV some pulsars such as the Crab, are among the brightest γ -ray sources in the sky. The EGRET detector, aboard the *Compton* γ -ray Observatory (CGRO), measured the spectra of different pulsars only up to $E \approx 5$ GeV, due to its small detector area (~ 0.1 m²) and decreasing fluxes at higher energies. Simple extrapolation of source spectra to higher energies makes them very promising targets for ground-based telescopes. At energies $E > 60$ GeV, Cherenkov telescopes¹ are the most sensitive instruments (3) because of the large detection area $\geq 10^4$ m². But, in spite of the numerous attempts over many years no pulsar has been detected so far by Cherenkov telescopes (4-9, 11, 12). This suggests a spectral cut-off between a few GeV and a few tens of GeV.

The Crab pulsar (PSR B0531+21), first discovered at radio frequencies in 1969 (13), is one of the best candidates for studying the cut-off. Its spectrum has been

¹ Gamma-rays induce particle air showers in the atmosphere that emit Cherenkov light. The detection of this light allows measuring the energy and the direction of the incident gamma-ray.

measured by EGRET (14) up to $E \approx 5$ GeV without a clear, significant cut-off being seen. Earlier observations of the Crab pulsar and the Crab nebula in 2006 by the 17 m diameter MAGIC (15) telescope (Canary Island of La Palma, 2200m a.s.l.) have revealed a hint of pulsed emission at the 2.9σ level above 60 GeV (12, 13). To verify this hint we have developed and installed a new trigger system that lowered the threshold of MAGIC from 50-60 GeV down to 25 GeV² (see supporting material).

We observed the Crab pulsar from October 2007 to February 2008, obtaining 22.3h of data under favorable observation conditions, and discovered pulsed emission above 25 GeV. In Fig. 2 we compare the measured pulsed γ -ray signal with our simultaneously recorded optical pulsation. Also we show the EGRET measurements above 100 MeV and above 1 GeV for the 33 ms rotation period of the Crab pulsar. The pulsed signal has an overall significance of 6.4σ with 8500 ± 1330 signal events. Phase zero is defined as the position of the main radio pulse (16). Our $E > 25$ GeV data show pronounced pulses at phase 0 (main pulse P1) and at phase 0.3-0.4 (inter pulse P2). These are coincident with those at lower energies $E > 100$ MeV and with those of our own optical measurement. We point out that P1 and P2 have about *equal* amplitudes at $E = 25$ GeV, in contrast to measurements at lower energies $E > 100$ MeV, where P1 is dominant. Our data show a small excess (3.4σ) above 60 GeV for P2 that is in accordance with our previous Crab observation (12, 13). Current satellite missions (AGILE (17), GLAST (18)) will need a few years to collect sufficient statistics at these energies, given the low fluxes.

For the Crab pulsar, EGRET (15) measured a power-law spectrum ($F(E) \propto E^{-\alpha}$ with $\alpha = 2.022 \pm 0.014$) in the energy range from $E = 0.1$ GeV to 5 GeV. At $E = 25$ GeV we measure a flux that is several times lower than a straightforward extrapolation of the EGRET spectrum. Obviously, a spectral cut-off sets in somewhere between 5 GeV and 25 GeV. Pulsar emission scenarios (1, 2) predict exponential ($F(E) \propto E^{-\alpha} \exp(-E/E_e)$) to super-exponential ($F(E) \propto E^{-\alpha} \exp(-(E/E_s)^2)$) shapes for the cut-off. E_e and E_s are the exponential and super-exponential cut-off energy parameters. To measure these, we extrapolate the P1+P2 phase-averaged EGRET energy spectrum to our energy band and introduce two cutoff scenarios, an exponential and a super-exponential one. The values of E_e and E_s are determined by matching the predicted number of signal events with the observed ones (Fig. 3a, 3b, 4). With the exponential assumption, we find a cutoff energy $E_e = 16.3 \pm 1.5_{\text{stat}} \pm 5.4_{\text{syst}}$ GeV. In the super-exponential case, we find $E_s = 20.7 \pm 1.5_{\text{stat}} \pm 5.7_{\text{syst}}$ GeV. The systematic error is dominated by a possible mismatch of the energy calibration between EGRET and MAGIC. The exponential fit is marginally preferred (Fig.3). Theoretical Crab pulsar models predict P1+P2 phase-averaged spectra (19, 20), which can then be compared with our result.

The spectral cutoff is explained as a combination of the maximum energies, ϵ_{max} , that electrons can reach – due to the balance between acceleration and radiation losses – and the absorption of the emitted γ -rays in the magnetosphere. The latter is controlled

² The threshold of a Cherenkov telescope is usually defined as the peak in the energy distribution of triggered gamma ray events for a gamma ray source with an $E^{-2.6}$ power law, photon energy spectrum.

by two mechanisms: *a)* magnetic e^+e^- pair production in the extremely strong magnetic field close to the pulsar surface, and *b)* photon-photon $\rightarrow e^+e^-$ pair production in dense photon fields. If, for a young pulsar with a magnetic field $B \sim 10^{12} - 10^{13}$ Gauss, emission occurs close to the NS surface (as in the classical *polar-cap* (1, 10, 21) and, to some extent, in *slot-gap* pulsar models (22, 23)), then magnetic pair-production attenuation provides a characteristic super-exponential cutoff at relatively low energies, i.e. a few GeV at most, with $\varepsilon_{\max} < 10$ GeV (1). If, on the other hand, emission occurs farther out in the magnetosphere, close to the light cylinder (as in *outer-gap* models (24, 25, 26)), then absorption mainly arises from photon-photon collisions, and the ensuing cutoff is shallower (exponential in shape), so γ -rays can escape (ε_{\max} is several tens of GeV). For a detailed discussion we refer to a review by Baring (1). His Eq. (1) - a largely model-independent relation, derived from simulations of γ -ray absorption by magnetic pair production in rotating magnetic dipoles - relates the pair-creation cutoff energy ε_{\max} with the location of the emission region r/R_0 (R_0 is the NS radius) for a NS with surface magnetic field B and period P :

$$\varepsilon_{\max} \approx 0.4 \sqrt{P \frac{r}{R_0}} \max \left\{ 1, \frac{0.1 B_{\text{crit}}}{B_0} \left(\frac{r}{R_0} \right)^3 \right\} \text{GeV}$$

The appropriate values for the Crab pulsar are: $B_0 = 8 \cdot 10^{12}$ Gauss (19), natural constant $B_{\text{crit}} = 4.4 \cdot 10^{13}$ Gauss and the period $P = 0.033$ s. Setting $\varepsilon_{\max} = E_s$ (E_s is the super-exponential cutoff energy of $E_s = 20.7 \pm 1.5_{\text{stat}} \pm 5.7_{\text{syst}}$ GeV derived above), one obtains an $r/R_0 = 5.9 \pm 0.13_{\text{stat}} \pm 0.44_{\text{syst}}$. This means that the emitting region is located well above the NS surface. This large distance seriously challenges the basic tenet of the *polar-cap* scenario (1, 10, 21) for the Crab, i.e. in which particle acceleration and emission of radiation should occur at very low altitudes (less than about one NS-radius (1) above the NS surface at the magnetic poles. Also, the high value of E_e considerably strains the *slot gap* scenario (19). Another prediction of the *polar-cap* scenario is a dependence of the pulse phases on energy (1). This appears to be ruled out by our observations, which show constant phases up to the highest energies.

In summary, the measured cut-off and the marginal preference for an exponential shape in the phase-averaged spectrum of the Crab pulsar suggest that the emitting region lies quite high above the NS surface, where the magnetic field strength and related pair creation rate are relatively low. This, together with the constancy of the pulse phase with photon energy, contradicts basic features of the *polar-cap* scenario (1). In addition, our present measurements reveal a trend of P2/P1 increasing with energy: it is < 0.5 at 100 MeV, ≈ 1 at 25 GeV, and > 1 at 60 GeV (Fig. 2). This tendency provides valuable information for theoretical studies that will further constrain the location in the magnetosphere where the emission takes place (see, for example, a recent *outer gap* model (20)).

Future observations will allow studies of the Crab pulsar with better statistics, revealing finer differences in the spectra of P1 and P2, especially at energies well above 40 GeV where current satellite detectors (AGILE (17), GLAST (18)) have low

sensitivity. Our observations clearly demonstrate that high sensitivity pulsar studies with low threshold air Cherenkov telescopes have become a reality. This ushers in a new era in ground-based very high energy γ -ray astrophysics.

References and Notes

1. Baring, M. G., *Adv. Space Res.*, 33, 552-560 (2004)
2. Cheng, K. S., *Adv. Space Res.*, 33, 561-570 (2004)
3. Daugherty, J.K. & Harding, *Astrophys. J.* 252, 337-347 (1982)
4. Chadwick, P. et al., *Astroparticle Physics*, 9, Is. 2, 131-136 (1998)
5. Edwards, P.G. et al., *Astronomy & Astrophysics*, 291, 468-472 (1994)
6. Aharonian, F. et al., *Astrophys. J.*, 614, 897-913 (2004)
7. De Naurois, M. et al., *Astrophys. J.*, 566, 343-357 (2002)
8. Lessard, R.W. et al., *Astrophys. J.*, 531, 942-948 (2000)
9. Aharonian, F. et al., *Astronomy & Astrophysics*, 466, 543-554 (2007)
10. Thompson, D.J., Bertsch, D.L. & O'Neal, R.H., *Astrophys. J. Suppl. Ser.*, 157, 324-334 (2005)
11. Albert, J. et al., *Astrophys. J.* 674, 1037-1055 (2008)
12. Otte, A.N., *PhD Thesis Technical University Munich 2007*, <http://nbn-resolving.de/urn/resolver.pl?urn:nbn:de:bvb:91-diss-20070924-620881-1-0>
13. Staelin, D. H. & Reifenstein, E. C., Pulsating Radio Sources near the Crab Nebula, *Science*, 162, 1481-1483 (1968)
14. Kuiper, L., Hermsen, W., et al., The Crab pulsar in the 0.75-30 MeV range as seen by CGRO COMPTEL. A coherent high-energy picture from soft X-rays up to high-energy gamma-rays, *Astronomy & Astrophysics*, 378, 918-935 (2001)
15. The MAGIC telescope website (<http://wwwmagic.mppmu.mpg.de>).
16. Jodrell Bank Radio Telescope website (<http://www.jb.mac.ac.uk/pulsar/crab.html>)
17. The AGILE satellite website (<http://agile.rm.iasf.cnr.it/>)
18. The GLAST telescope website (<http://www-glast.stanford.edu>).
19. Harding, A.K., Stern, J.V., Dyks, J. & Frackowiak, F., High-Altitude Emission from Pulsar Slot Gaps: The Crab Pulsar, *Astrophys. J.* 680, 1378-1393 (2008)
20. Tang, A.P.S., Takata, J., Jia, J. & Cheng, K.S., A Re-Visit of of the Phase resolved X-ray and γ -ray Spectra of the Crab Pulsar, *Astrophys. J.* 676, 562-572 (2008)
21. Ruderman, M. A., Sutherland, P. G., Theory of pulsars- Polar caps, sparks, and coherent microwave radiation, *Astrophys. J.*, 196, 51-72 (1975)
22. Muslimov, A.G. & Harding, A.K., *Astrophys. J.* 606, 1143-1153 (2004)

23. Arons, J., Scharlemann, E.T., *Astrophys. J.* 231, 854-879 (1979)
24. Cheng, K.S., Ho, C. & Ruderman, M., *Astrophys. J.* 300, 500-521 (1986)
25. Hirotani, K., *Astrophys. J.*, 662, 1173-1176 (2007)
26. Romani, R.W., *Astrophys. J.*, 470, 469-478 (1996)
27. Goldreich, P. & Julian, *Astrophys. J.* 157, 869-880 (1969)
28. Data provided by EGRET (<ftp://legacy.gsfc.nasa.gov/compton/data/egret/>)
29. Lucarelli, F, Barrio, J. A., Antoranz, P. et al., *Nucl. Instr. Meth. A*, 589, 415-424 (2008)

30. We want to thank the electronics division at the MPI, Munich, for their enthusiastic work in developing and producing the new analogue sum trigger system, especially Olaf Reimann, Ronald Maier, Si Tran and Toni Dettlaff. We also thank Leo Stodolsky for critical reading of the manuscript. We would like to thank the Instituto de Astrofísica de Canarias for the excellent working conditions at the Observatorio del Roque de los Muchachos in La Palma. The support of the German BMBF and MPG, the Italian INFN and INAF, the Swiss SNF and Spanish MCINN is gratefully acknowledged. This work was also supported by ETH Research Grant TH 34/043, by the Polish MNiSzW Grant N N203 390834, and by the YIP of the Helmholtz Gemeinschaft.

List of Authors and Affiliations

E. Aliu¹, H. Anderhub², L. A. Antonelli³, P. Antoranz⁴, M. Backes⁵, C. Baixeras⁶, J. A. Barrio⁴, H. Bartko⁷, D. Bastieri⁸, J. K. Becker⁵, W. Bednarek⁹, K. Berger¹⁰, E. Bernardini¹¹, C. Bigongiari^{8,30}, A. Biland², R. K. Bock^{7,8}, G. Bonnoli¹², P. Bordas¹³, V. Bosch-Ramon¹³, T. Bretz¹⁰, I. Britvitch², M. Camara⁴, E. Carmona⁷, A. Chilingarian¹⁴, S. Commichau², J. L. Contreras⁴, J. Cortina¹, M. T. Costado^{15,16}, S. Covino³, V. Curtef⁵, F. Dazzi⁸, A. De Angelis¹⁷, E. De Cea del Pozo¹⁸, R. de los Reyes⁴, B. De Lotto¹⁷, M. De Maria¹⁷, F. De Sabata¹⁷, C. Delgado Mendez¹⁵, A. Dominguez¹⁹, D. Dorner¹⁰, M. Doro⁸, D. Elsässer¹⁰, M. Errando¹, M. Fagiolini¹², D. Ferenc²⁰, E. Fernandez¹, R. Firpo¹, M. V. Fonseca⁴, L. Font⁶, N. Galante⁷, R. J. Garcia Lopez^{15,16}, M. Garczarczyk⁷, M. Gaug¹⁵, F. Goebel⁷, D. Hadasch⁵, M. Hayashida⁷, A. Herrero^{15,16}, D. Höhne¹⁰, J. Hose⁷, C. C. Hsu⁷, S. Huber¹⁰, T. Jogler⁷, D. Kranich², A. La Barbera³, A. Laille²⁰, E. Leonardo¹², E. Lindfors²¹, S. Lombardi⁸, F. Longo¹⁷, M. Lopez⁸, E. Lorenz^{2,7}, P. Majumdar⁷, G. Maneva²², N. Mankuzhiyil¹⁷, K. Mannheim¹⁰, L. Maraschi³, M. Mariotti⁸, M. Martinez¹, D. Mazin¹, M. Meucci¹², M. Meyer¹⁰, J. M. Miranda⁴, R. Mirzoyan⁷, M. Moles¹⁹, A. Moralejo¹, D. Nieto⁴, K. Nilsson²¹, J. Ninkovic⁷, N. Otte^{23,7,29}, I. Oya⁴, R. Paoletti¹², J. M. Paredes¹³, M. Pasanen²¹, D. Pascoli⁸, F. Pauss², R. G. Pegna¹², M. A. Perez-Torres¹⁹, M. Persic²⁵, L. Peruzzo⁸, A. Piccioli¹², F. Prada¹⁹, E. Prandini⁸, N. Puchades¹, A. Raymers¹⁴, W. Rhode⁵, M. Ribó¹³, J. Rico^{26,1}, M. Rissi², A. Robert⁶, S. Rügamer¹⁰, A. Saggion⁸, T. Y. Saito⁷, M. Salvati³, M. Sanchez-Conde¹⁹, P. Sartori⁸, K. Satalecka¹¹, V. Scalzotto⁸, V. Scapin¹⁷, T. Schweizer⁷, M. Shayduk⁷, K. Shinozaki⁷, S. N. Shore²⁴, N. Sidro¹, A. Sierpowska-Bartosik¹⁸, A. Sillanpää²¹, D. Sobczynska⁹, F. Spanier¹⁰, A. Stamerra¹², L. S. Stark², L. Takalo²¹, F. Tavecchio³, P. Temnikov²², D. Tescaro¹,

M. Teshima⁷, M. Tluczykont¹¹, D. F. Torres^{26,18}, N. Turini¹², H. Vankov²², A. Venturini⁸, V. Vitale¹⁷,
 R. M. Wagner⁷, W. Wittek⁷, V. Zabalza¹³, F. Zandanel¹⁹, R. Zanin¹, J. Zapatero⁵,
 (MAGIC collaboration)
 O.C. de Jager²⁷, E. de Ona Wilhelmi^{1,28}

Correspondence and request of materials to Thomas Schweizer <tschweiz@mppmu.mpg.de> ,
 Nepomuk Otte <otte@mppmu.mpg.de>, Michael Rissi, <Michael.Rissi@phys.ethz.ch>,
 Maxim Shayduk <shayduk@mppmu.mpg.de>, Marcos Lopez Moya <marcos.lopezmoya@pd.infn.it>

1. IFAE, Edifici Cn., Campus UAB E-08193 Bellaterra, Spain, 2. ETH, Zürich, CH-8093 Switzerland, 3.
 INAF, I-00136 Rome, Italy, 4. Universidad Complutense E-28040 Madrid, Spain, 5. Technische
 Universität Dortmund, D-44221 Dortmund, Germany, 6. Universitat Autònoma de Barcelona, E-08193
 Bellaterra, Spain, 7. Max-Planck-Institut für Physik, D-80805 München, Germany, 8. Università di
 Padova and INFN, I-35131 Padova, Italy, 9. University of Lodz, PL-90236 Lodz, Poland, 10. Universität
 Würzburg D-97074 Würzburg, Germany, 11. DESY Deutsches Elektr.-Synchrotron,
 D-15738 Zeuthen, Germany, 12. Università di Siena and INFN Pisa, I-53100 Siena, Italy, 13. Universitat
 de Barcelona (ICC/IEEC), E-08028 Barcelona, Spain, 14. Yerevan Physics Institute, AM-375036
 Yerevan, Armenia, 15. IAC, E-38200, La Laguna, Tenerife, Spain, 16. Depto. de Astrofísica, Universidad,
 E-38206 La Laguna, Tenerife, Spain, 17. Università di Udine and INFN Trieste, I-33100 Udine, Italy, 18.
 IEEC-CSIC, E-08193 Bellaterra, Spain, 19. CSIC, E-18080 Granada, Spain, 20. Davis University of
 California, CA-95616-8677, USA, 21. Tuorla Observatory, Turku University, FI-21500 Piikkiö, Finland,
 22. Inst. for Nucl. Research and Nucl. Energy, BG-1784 Sofia, Bulgaria, 23. Humboldt-Universität zu
 Berlin, D-12489 Berlin, Germany, 24. Università di Pisa and INFN Pisa, I-56126 Pisa, Italy, 25.
 INAF/Osservatorio Astronomico and INFN, I-34143 Trieste, Italy, 26. ICREA, E-08010 Barcelona,
 Spain. 27. Unit for Space Physics, Northwest University, Potchefstroom 2520, South Africa 28. Now at
 Astroparticule et Cosmologie, CNRS, Universite Paris, F-75205 Paris Cedex 13, 29. Now at Santa Cruz
 Institute for Particle Physics, University of California, Santa Cruz, CA 95064, USA, 30. Now at IFIC -
 Instituto de Física Corpuscular , CSIC-UVEG, E-46071 Valencia, Spain

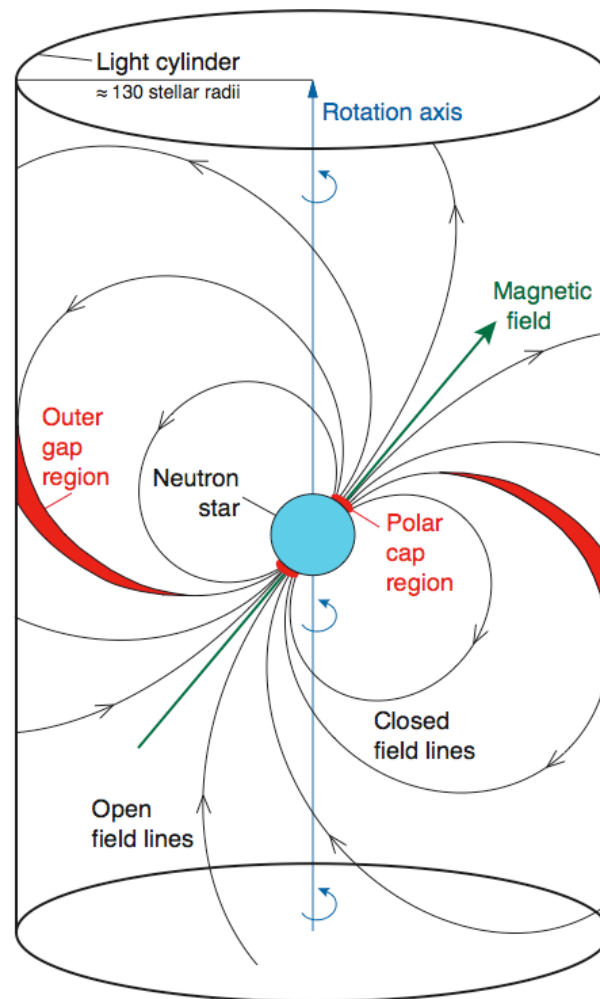


Figure 1: A sketch of the Crab pulsar's magnetosphere: Electrons are trapped and accelerated along the magnetic field lines of the pulsar and emit electromagnetic radiation via the synchrotron-curvature radiation mechanism. Vacuum gaps or vacuum regions occur at the polar cap (1), very close to the neutron star surface, and in the outer region (2) close to the light cylinder (outer gap regions). Vacuum gaps are filled with plasma, but its density is lower than the critical Goldreich-Julian density (28), at which the magnetically induced electric field is saturated, and therefore electrons can be accelerated to very high energies. Absorption of high-energy γ -rays occurs by interaction with the magnetic field (magnetic pair production) as well as with the photon field (photon-photon pair production). The former dominates close to the surface of the neutron star where the magnetic field is strongest. It leads to a super-exponential cutoff at relatively low energies (few GeV). Photon-photon collisions prevail farther out in the magnetosphere close to light cylinder, where the magnetic field is lower, and lead to an exponential cutoff at higher (>10 GeV) energies.

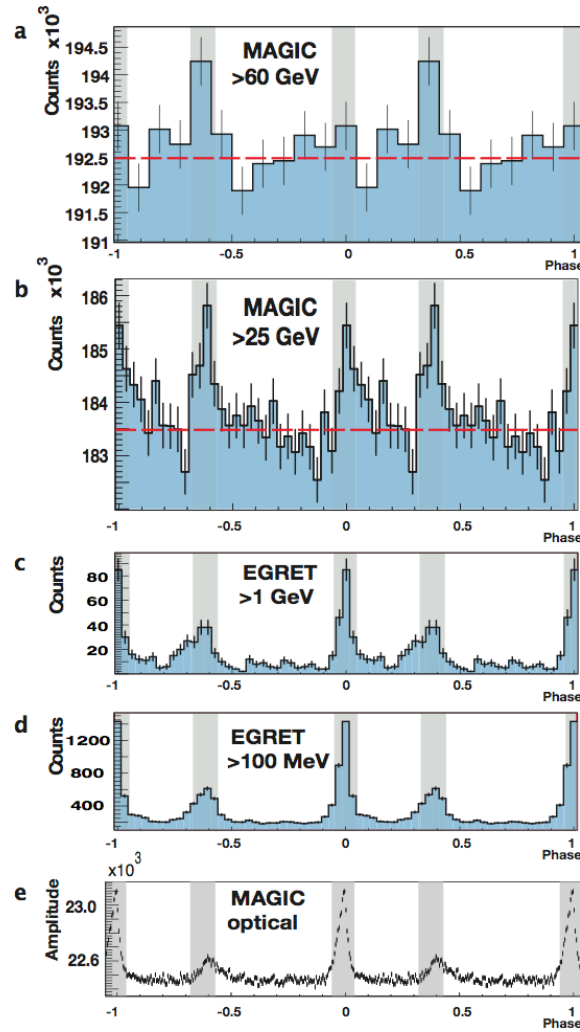
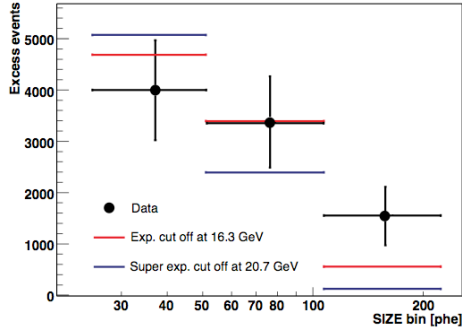


Figure 2: Pulsed emission in different energy bands. The shaded regions show the signal regions for the main pulse (P1) and the secondary pulse (P2). From top to bottom: Panel *a*: Evidence of an emission (3.4σ) above 60 GeV for P2 measured by MAGIC; Panel *b*: Emission ≥ 25 GeV measured by MAGIC; Panel *c*: Emission ≥ 1 GeV measured by EGRET (28); Panel *d*: Emission ≥ 100 MeV measured by EGRET (28); Panel *e*: Optical pulsations measured by MAGIC (9, 20). The optical signal has been recorded simultaneously with the γ -rays. P1 and P2 are in phase for all shown energies. The figure illustrates how the ratio of P2/P1 increases with energy in the panels *b-d*. In search for pulsed emission, the arrival time of each event, after correcting for the solar system barycenter, was transformed into the phase of the rotational period of the neutron star. The significance of the γ -ray pulsation above 25 GeV was evaluated by a single-hypothesis test (described in the supporting material), where the γ -ray emission was assumed coming from the two fixed phase intervals (shaded regions): P1 (phase 0.94 to 0.04) and P2 (phase 0.32 to 0.43), as defined in (13, 15). The signal results in 8500 ± 1330 signal events (6.4σ).

a



b

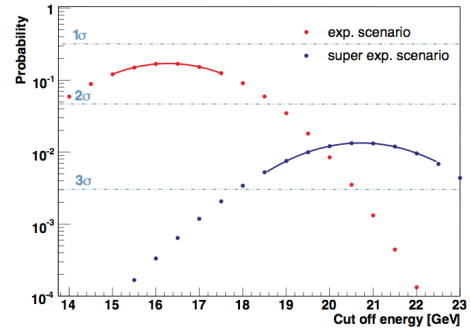


Figure 3: Model fits to the signal event distribution. Panel *a* shows the measured SIZE distribution of the P1+P2 phase-integrated signal. SIZE is a main image parameter, which measures the total intensity of the Cherenkov flash in the camera (in units of photoelectrons). In this analysis it is used as a rough estimate of the γ -ray energy. To measure the cutoff, we extrapolate the P1+P2 phase-averaged EGRET (15) energy spectrum to our energy band and introduce two cutoff scenarios, a) an exponential cutoff: $F(E) \propto E^\alpha \exp(-E/E_c)$ (red bins) and b) a super-exponential cutoff: $F(E) \propto E^\alpha \exp(-(E/E_s)^2)$ (blue bins). Then we estimate the expected number of signal events in each SIZE bin by folding the extrapolated spectrum with the MAGIC effective area. The figure shows the best-fit solution for the exponential and the super-exponential case. Panel *b* shows the probability curves calculated from the χ^2 -test for the model to the data with cutoffs at different energies. The red curve corresponds to the exponential model, the blue curve to the super-exponential model. The most probable cutoff energies are: $16.3 \pm 1.5_{\text{stat}} \pm 5.4_{\text{sys}}$ GeV for the exponential model, and $20.7 \pm 1.5_{\text{stat}} \pm 5.7_{\text{sys}}$ GeV for the super-exponential model.

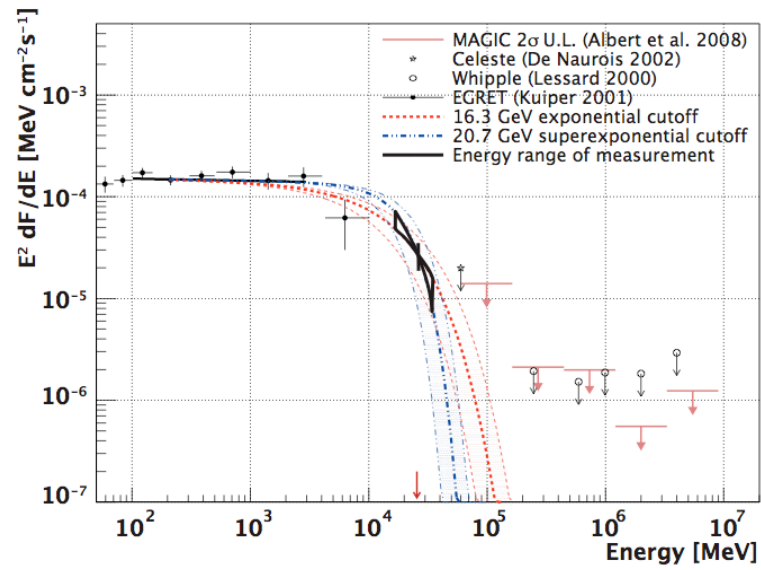


Figure 4: Crab pulsar spectral cutoff. The black flux point indicates the energy range and the statistical error of our flux measurement, assuming an exponential and a super-exponential cut-off. The black crosses on the left represent flux measurements from EGRET (15). The arrows on the right denote upper limits from various previous experiments. The EGRET spectrum has been extrapolated with an exponential (red) and a super-exponential (blue) shape. The coloured bands illustrate the combined statistical and systematic errors and denote the total uncertainty of our measurement, by which the flux point can move to higher or lower energies.